XPENG ROBOTICS

Athena-WBC: Capability-Aligned Policy Experts for Long-Tail Humanoid Whole-Body Control

Yuan Jiang*, Ningyuan Zhang*, Xicun Yang, Yuzhi Jiang, Jie Chen†

XPENG Robotics

Abstract

Large-scale humanoid motion-tracking controllers are commonly improved by reallocating training effort: difficult motions are sampled more often, isolated into smaller subsets, or assigned to specialized experts. We show that this view is incomplete. In strong whole-body-control baselines, a residual set of feasible training clips remains unsolved even under targeted training, especially for high-dynamic transitions and balance-critical motions. These failures arise not only from insufficient exposure, but from a mismatch between the motion demands and the effective capability induced by the default training recipe.

We propose *Athena-WBC*, a compact teacher-student pipeline with capability-aligned policy experts for long-tail humanoid whole-body control. Dynamic experts use a tracking-focused, constraint-aware objective that removes conservative effort and temporal-control penalties while preserving physical feasibility constraints; balance experts use a gravity curriculum to improve early-training survivability. The resulting privileged teachers are motion-routed for DAgger distillation and then compressed into a single controller with deployable observations followed by RL fine-tuning. Experiments on a full-size humanoid show improved recovery of training-set long-tail motions and better held-out tracking than a strong SONIC-recipe baseline, using only a small number of experts.

1 Introduction

Humanoid whole-body control (WBC) has progressed from tracking isolated skills to imitating large and diverse human motion corpora [1–3]. Modern motion-conditioned policies can achieve high aggregate tracking performance by combining reinforcement learning, motion tracking rewards, privileged teacher policies, and deployable student distillation. However, high average performance does not imply that the training distribution has been fully absorbed. In particular, the high-coverage regime exposes a residual training-set long tail: motions that appear in the training corpus but remain unsolved by the learned controller. This failure mode is distinct from generalization failure and has received comparatively less attention.

We observe this phenomenon in the SONIC baseline. As shown in Fig. 2, evaluating the released SONIC checkpoint on its training motion set leaves a small but meaningful fraction of clips unsuccessful. These failures are not uniformly distributed. They concentrate in high-dynamic transitions, such as rapid direction changes and aggressive contact switches, and in balance-critical motions, such as low-support poses and slow recovery phases. Moreover, in our own controlled experiments, we find that a subset of failures persists even when the policy is trained only on the failed clips. This suggests that the default training recipe can induce an effective capability bottleneck rather than merely suffering from insufficient exposure to rare motions.

A common response to long-tail failures is to reallocate training effort: sample difficult motions more frequently [1, 4–9], cluster motions into narrower subsets [10], or train larger banks of specialized

* Equal contribution: Yuan Jiang and Ningyuan Zhang.
† **Correspondence:** Jie Chen at chenj81@xiaopeng.com

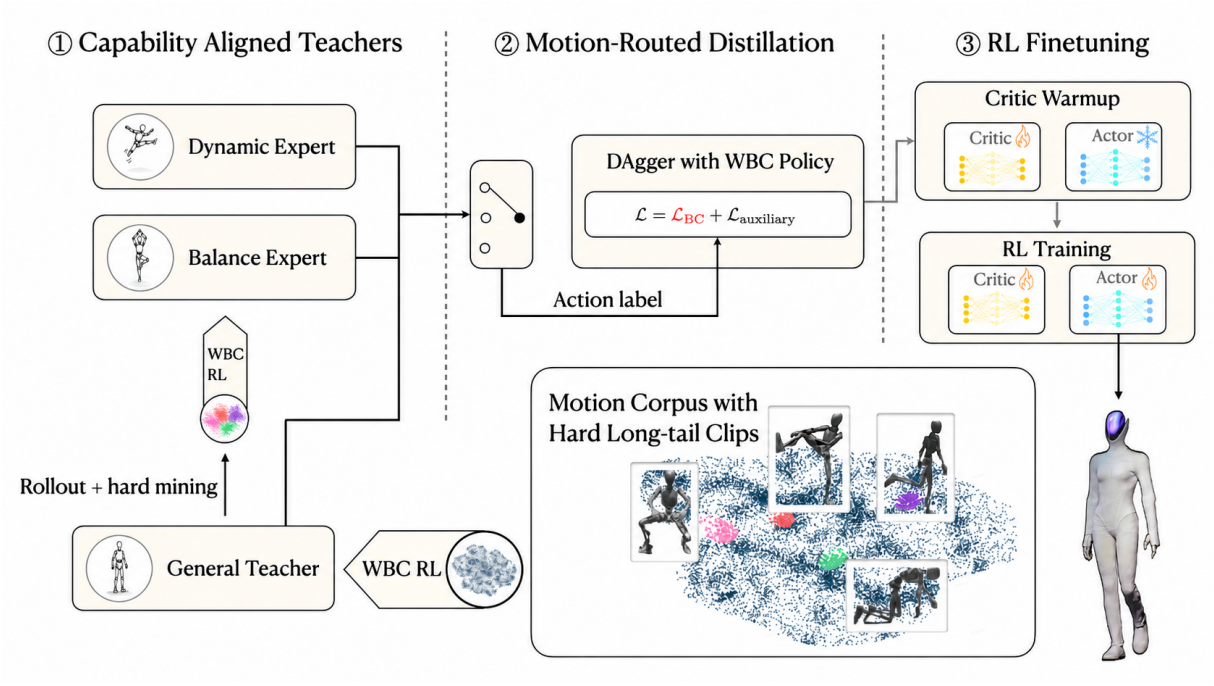

Figure 1: Overview of *Athena-WBC*. A general privileged teacher is trained on the full motion set. Residual failures are mined and used to train dynamic and balance experts in parallel. The frozen teachers are then routed per motion, distilled into a single student, and finetuned with RL.

experts [11]. These strategies can improve coverage, but they primarily change which data a policy sees. They do not necessarily change the control regime that the policy is encouraged to acquire. For high-dynamic motions, standard effort and temporal-smoothness penalties can suppress aggressive but feasible actuation. For balance-critical motions, early training under nominal gravity can terminate before the policy experiences informative tracking states. Thus, some residual failures require adapting the learning capability of the assigned expert, not only reallocating the data assigned to it.

We propose *Athena-WBC*, a compact teacher-student pipeline for long-tail humanoid WBC. For high-dynamic residual motions, we train dynamic experts with a tracking-focused and constraint-aware objective: tracking rewards and physical constraint penalties are retained, while effort and temporal-control penalties are removed from the reward. Smoothness is instead imposed through auxiliary policy regularization, allowing large but structured action changes. For balance-critical residual motions, we train balance experts with a gravity curriculum that improves early-training survivability before restoring nominal dynamics. The resulting privileged experts are evaluated on the training set, routed per motion according to rollout performance, distilled into a single student with DAgger-style supervision [12], and finally finetuned with RL to improve closed-loop tracking and deployment quality.

We evaluate the proposed pipeline in the high-coverage setting where residual failures, threshold sensitivity, and motion-specific tracking fidelity matter. In addition to standard success rate and tracking errors such as MPJPE, we report threshold-sensitive diagnostics through a Success–Tolerance Curve (STC) and Threshold-Integrated Success (TIS), and salience-aware tracking through Motion-Salience Weighted MPJPE (MPJPE-W). These metrics complement the standard single-threshold evaluation and make visible whether improvements come from better average tracking, stronger long-tail robustness, or more accurate tracking of the motion-defining body parts.

Our contributions are:

- We identify training-set long-tail failure as a capability bottleneck in humanoid WBC: some hard motions remain unsolved even under targeted exposure, especially in high-dynamic and balance-critical regimes.
- We propose *Athena-WBC*, a compact teacher-student pipeline that trains dynamic and balance

experts with capability-specific objectives and curricula, then distills them into one policy with deployable observation interface.

- We provide a comprehensive long-tail tracking evaluation with both standard metrics and threshold- and salience-aware diagnostics, showing that the final policy improves residual training-motion recovery and held-out tracking over a strong SONIC-recipe baseline (SONIC-Base).

2 Related Work

General humanoid motion tracking and scaling. Learning-based humanoid whole-body control has increasingly been formulated as large-scale physics-based motion tracking over human motion corpora. PHC learns a scalable humanoid controller for large motion sets and includes recovery from fail states [2]. OmniH2O uses kinematic pose as a universal interface for human-to-humanoid teleoperation and autonomy, and trains deployable students from privileged teachers [3]. Recent systems further scale this recipe in data, architecture, and training compute. GMT proposes a general motion-tracking framework for humanoid WBC [13]; EGM improves efficiency for high-dynamic tracking through adaptive curricula and specialized architectural choices [4]; SONIC scales model capacity, data volume, and training compute to build a natural humanoid whole-body tracker [1]; and Humanoid-GPT studies GPT-style Transformer scaling on a billion-scale motion corpus for zero-shot motion tracking [11]. These works show that scaling is a powerful route to general tracking. Our work studies a complementary question: even when a strong WBC pipeline has access to the training motions, why do feasible long-tail clips remain unsolved, and how should the training infrastructure be changed to acquire them?

Data allocation and motion partitioning for long-tail coverage. A common strategy for improving long-tail coverage is to reorganize the training distribution. Difficulty-aware sampling methods estimate which motions or segments are underlearned and allocate more rollout budget to them; GMT uses adaptive sampling together with motion mixture-of-experts modules [13], EGM uses bin-level tracking statistics to construct a cross-motion curriculum [4], and ZEST focuses training on difficult motion segments as part of an athletic skill-transfer pipeline [14]. Another line partitions the motion corpus and trains specialized experts before distilling them into a generalist policy. BumbleBee clusters motions using semantic and kinematic features, trains cluster-specific experts, and distills them into a unified whole-body controller [10]. These methods are effective mechanisms for reducing data imbalance or interference across motion types, but they share an implicit assumption: once a difficult motion receives enough training budget or is assigned to a sufficiently specific subset, the standard acquisition recipe should be capable of learning it. Our results show that this assumption can fail. A policy may still fail to overfit a feasible hard clip if its acquisition recipe lacks the physical capability required by that motion. We therefore align experts by capability, rather than treating long-tail recovery purely as sampling or motion partitioning.

Physically consistent references and motion feasibility. Physically consistent reference generation provides another route to hard-motion tracking. OmniTrack is an especially important comparison because it reports a result that partially contrasts with ours: after generating physically feasible robot references, a single deployable PPO tracker can cover a wide range of high-dynamic and contact-rich motions without DAgger-style teacher-action supervision [15]. Its key intervention is upstream of the final tracker. OmniTrack first trains a privileged PPO-based physical-motion generation policy with simulator-side observations to roll out dynamics-consistent robot trajectories from raw retargeted references. These rollouts are stored as new references, including joint states, global states, velocities, orientations, and contact information; the final tracker is then trained with PPO on these generated references, using deployment-oriented noise and domain randomization. Thus, OmniTrack shows that, for some embodiments and datasets, reference correction plus a strong physical-motion generation stage can remove much of the apparent long-tail difficulty. Our results differ. On our full-size 80 kg humanoid with planetary-roller-screw actuation and closed-chain mechanisms, we observe persistent training-set

long-tail failures under SONIC-Base, and even an OmniTrack-style single physical-motion generation stage does not reliably acquire the hardest clips. We therefore treat OmniTrack as a complementary and partially contradictory result: it demonstrates the power of reference-level correction, while our work studies the remaining regime where embodiment difficulty and policy capability bottlenecks require capability-aligned experts for high-dynamic and balance-critical motions.

Regularization and deployable control quality. Deployable humanoid control requires more than accurate tracking: actions should avoid high-frequency chatter, excessive torque variation, and extreme control outputs. Many WBC pipelines therefore include regularization rewards on action magnitude, action rate, torque, torque rate, joint velocity, or joint acceleration. These terms improve nominal actuation quality but can also reshape the RL objective and suppress the aggressive controls required by high-dynamic motions. CAPS regularizes policies through temporal and spatial action losses [16], while Grad-CAPS penalizes changes in the action gradient to improve the expressiveness–smoothness trade-off [17]. More general policy regularizers, including weight decay, have also been studied in continuous-control policy optimization [18, 19]. Our work studies where such regularization should enter long-tail expert acquisition. We keep tracking rewards and physical constraint penalties, such as joint-limit, velocity-limit, torque-limit, and foot-slip penalties, but remove energy/effort and temporal-control penalties during dynamic expert training. We then recover control smoothness through auxiliary policy regularization rather than reward-level conservatism.

Curricula, expert distillation, and fine-tuning. Curriculum and assistance mechanisms are widely used to make difficult locomotion and motion-imitation tasks learnable. Residual Force Control augments humanoid policies with external residual forces to imitate agile or physically mismatched motions [20]; ZEST uses a model-based assistive-wrench curriculum together with adaptive sampling to learn dynamic, long-horizon skills [14]; and A2CF learns adaptive assistive curriculum forces for humanoid motion learning [21]. Our gravity curriculum follows the same continuation-learning principle but uses gravity scale as the curriculum variable, directly targeting the cold-start survival problem of balance-critical motions. After expert acquisition, we use standard expert-to-student compression: DAgger mitigates distribution shift by collecting learner-induced states and labeling them with expert actions [12]. We also follow the distillation–fine-tuning recipe of Parkour in the Wild, which trains terrain-specific experts, distills them with DAgger, and then improves the unified policy through RL fine-tuning [22]. Our contribution is not a new distillation algorithm; rather, we use this compression and fine-tuning machinery to turn a compact set of capability-aligned humanoid WBC experts into a single controller with deployable observations, and we find that post-distillation RL fine-tuning is vital for motion generalization.

3 Problem Formulation

3.1 Motion-Conditioned Humanoid Whole-Body Control

Let

$$\mathcal{D}_{\text{train}} = \{\tau_m\}_{m=1}^{M}. \tag{1}$$

denote a fixed training set of reference motion clips. Each clip τ_m specifies a target humanoid trajectory over time. At time t, a motion-conditioned controller receives an observation o_t containing the current robot state and reference-tracking target, and outputs an action a_t for whole-body control. The policy is trained to maximize the expected discounted return

$$\max_{\theta} \mathbb{E}_{\tau_m \sim \mathcal{D}_{\text{train}},\, \pi_\theta} \left[\sum_t \gamma^t r_t \right]. \tag{2}$$

We decompose the reward into tracking rewards and three additional reward components:

$$r_t = r_t^{\text{track}} + r_t^{\text{phys}} + r_t^{\text{effort}} + r_t^{\text{temp}}. \tag{3}$$

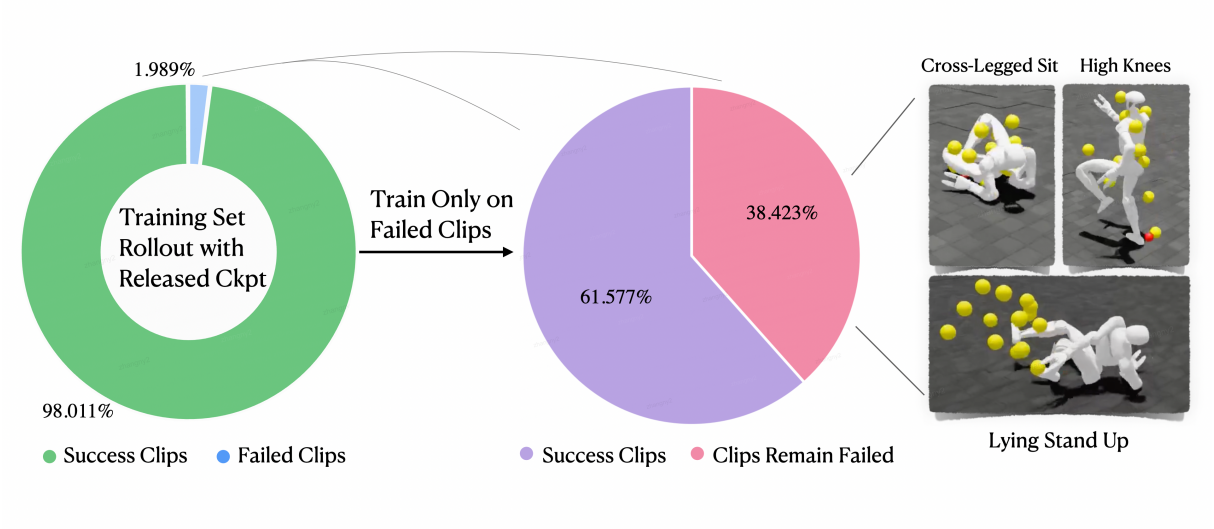

Figure 2: Training-set long-tail failures in SONIC baseline. The released checkpoint leaves a small but non-negligible fraction of Bones-Seed training clips unsuccessful. Targeted retraining recovers many failures, but residual cases concentrate in high-dynamic and balance-critical regimes, with some cases attributable to data artifacts or apparent physical saturation.

Here r_t^{track} measures imitation quality, including root, joint, and key-body tracking. The physical-constraint reward r_t^{phys} contains feasibility-related penalty terms, such as joint-position-limit, joint-velocity-limit, torque-limit, and foot-slip penalties. Although written as a reward component, r_t^{phys} is typically non-positive and discourages physically invalid or unsafe behavior.

The effort reward r_t^{effort} contains energy and actuation regularization terms, such as torque-magnitude, DoF-velocity, and DoF-acceleration penalties. The temporal-control reward r_t^{temp} contains action-rate, torque-rate, and action-smoothness penalties. These terms are also usually non-positive. They are useful for encouraging conservative, smooth, and hardware-suitable control, but they also bias the policy toward low-effort and low-rate actions. This bias can be undesirable for motions that require rapid momentum changes, aggressive contact transitions, or large but feasible actuation.

This decomposition motivates the central distinction used in this paper: r_t^{phys} encodes physical feasibility, whereas r_t^{effort} and r_t^{temp} encode conservative control preferences. Treating all three as interchangeable regularization can limit the effective capability of the learned controller, especially in high-dynamic long-tail regimes.

3.2 Training-Set Residual Coverage

We study the high-coverage regime, where the goal is not only to generalize to unseen motions, but also to absorb as much of the training distribution as possible. Let

$$S(\pi, \tau_m) \in \{0, 1\} \tag{4}$$

be a binary success predicate indicating whether policy π successfully tracks clip τ_m under the evaluation protocol. The training-set coverage of π is

$$C(\pi; \mathcal{D}_{\text{train}}) = \frac{1}{M} \sum_{m=1}^{M} S(\pi, \tau_m). \tag{5}$$

Given a baseline policy π_0, we define its residual failure set as

$$\mathcal{R}(\pi_0) = \{\tau_m \in \mathcal{D}_{\text{train}} \ : \ S(\pi_0, \tau_m) = 0\}. \tag{6}$$

The objective of this work is to improve coverage on $\mathcal{R}(\pi_0)$ while preserving performance on the full training distribution and on held-out motions. We focus on residual clips that are recoverable under the target embodiment and nominal evaluation dynamics. Clips dominated by data artifacts or clear physical infeasibility are treated separately in the analysis rather than as failures of the controller alone.

3.3 Capability Bottleneck

A common approach to improving long-tail coverage is to modify data allocation: difficult clips are sampled more often, grouped into narrower subsets, or assigned to specialized experts. These strategies change which motions a policy sees, but often leave the acquisition recipe unchanged.

We use *capability* to denote the class of motions that a policy can reliably acquire under a fixed robot embodiment, evaluation protocol, and acquisition recipe. The acquisition recipe includes the teacher observation, reward design, curriculum, policy class, optimizer, and training budget. We say that a residual clip exposes a *capability bottleneck* when it remains unsolved after data-only interventions under the baseline recipe, such as oversampling or training on the failed subset, but becomes solvable after changing capability-relevant parts of the recipe. The bottleneck is therefore not merely that the motion was rare or under-sampled; it is that the default recipe induces an effective control regime that is mismatched to the motion.

This definition is operational and relative to the embodiment, simulator, evaluation protocol, and training budget. A clip that is recovered by additional sampling is treated as a data-allocation failure. A clip dominated by annotation artifacts or clear physical infeasibility is treated separately. The regime of interest here is the remaining set: feasible residual motions that require changing how the expert is trained, not only how often the motion is presented.

The reward decomposition above illustrates two such bottlenecks. For high-dynamic motions, effort and temporal-control penalties can suppress aggressive but physically feasible actions. For balance-critical motions, early policies may fall under nominal gravity before reaching informative tracking states. These regimes require different capability interventions: dynamic motions benefit from a less conservative acquisition objective, while balance-critical motions benefit from a curriculum that improves early survivability. Athena-WBC addresses residual coverage by adapting the capability of the assigned experts and then compressing those experts into a single controller.

4 Method

Figure 1 summarizes our pipeline. We first train a general privileged teacher on the full motion set. We then mine its residual failure set and train two capability-aligned experts, one dynamic and one balance expert, on that same residual set. Finally, we route each training motion to the best frozen teacher, distill the routed teachers into one student, and finetune the student with RL.

4.1 Two-Round Capability-Aligned Teacher Training

Our teacher design is inspired by the privileged motion-tracking experts used in omniH2O [3]: teachers are trained with access to clean simulator and reference-tracking features, and their behavior is later transferred to a student that uses only deployable observations.

Unlike iterative expert-mining pipelines that repeatedly retrain new experts on newly discovered failures, we use only two teacher-training rounds. This keeps the teacher bank compact and avoids many loops of expert training.

Round 1: general teacher. We first train a general teacher π_T^{gen} on the full training motion set $\mathcal{D}_{\text{train}}$. After training, we evaluate it on every training clip using multiple stochastic rollouts. Let K_{eval} denote

Table 1: Observation spaces used in our R02 SONIC experiments.

Observation block	**SONIC-Base**	**SONIC-Obs Teacher**	**OmniH2O Teacher**	**Expert Teacher**	**Student**
Robot target, 10 frames (340)	×	×	×	×	×
Hybrid target, (281)	×	×	×	×	×
Human target, 10 frames (650)	×	×	×	×	×
Proprio history, 10 frames (810)	×	×			×
Privileged sim state (33)		×			
OmniH2O teacher self obs (205)			×	×	
OmniH2O teacher task obs (338)			×	×	
OmniH2O teacher prev-action (23)			×	×	
Actor obs dim	**2081**	**2114**	**1837**	**1837**	**2081**

Table 2: Reward components used by different training stages and ablation variants.

Component	**SONIC-Base**	**OmniH2O Teacher**	**Expert Teacher**	**NoSmooth**	**CAPS**	**Grad-CAPS**	**Student RLFT**
Tracking	×	×	×	×	×	×	×
Limit/contact	×	×	×	×	×	×	×
Smoothness	×	×					

the number of evaluation rollouts per clip. In our experiments, $K_{\text{eval}} = 10$. For any teacher policy π and clip τ_m, we define

$$\widehat{\text{SR}}(\pi, \tau_m) = \frac{1}{K_{\text{eval}}} \sum_{i=1}^{K_{\text{eval}}} S(\pi, \tau_m, i)\,, \tag{7}$$

where $S(\pi, \tau_m, i) \in \{0, 1\}$ indicates whether rollout i of policy π successfully tracks clip τ_m under the evaluation predicate.

We define the residual failure set as

$$\mathcal{R}_{\text{gen}} = \left\{ \tau_m \in \mathcal{D}_{\text{train}} : \widehat{\text{SR}}(\pi_T^{\text{gen}}, \tau_m) < \rho_{\text{fail}} \right\}, \tag{8}$$

with $\rho_{\text{fail}} = 0.8$ in our experiments. Thus, a clip is considered a failure if the general teacher succeeds in fewer than 80% of its evaluation rollouts.

Round 2: dynamic and balance experts. We then train two additional teachers on the same residual set $\mathcal{R}_{\text{gen}}$:

$$\Pi_T = \left\{ \pi_T^{\text{gen}}, \pi_T^{\text{dyn}}, \pi_T^{\text{bal}} \right\}. \tag{9}$$

The dynamic expert π_T^{dyn} and balance expert π_T^{bal} are not obtained through further iterative mining. Both see the same residual motions, but use different acquisition recipes. The dynamic expert targets motions requiring aggressive transitions and large but feasible control responses. The balance expert targets motions where early survivability and low-support stabilization are the dominant difficulty. Which expert ultimately supervises each motion is decided later by rollout-based routing, not by a fixed manual assignment.

Dynamic expert. For high-dynamic residual motions, the main issue is conservative control. Using the reward decomposition in Sec. 3.1, the dynamic expert is trained with

$$r_t^{\text{dyn}} = r_t^{\text{track}} + r_t^{\text{phys}}, \qquad r_t^{\text{effort}} = 0, \qquad r_t^{\text{temp}} = 0. \tag{10}$$

Thus, tracking rewards and physical-constraint penalties are retained, while effort and temporal-control penalties are removed from the reward. The retained physical terms include joint-position-limit, joint-velocity-limit, torque-limit, and foot-slip penalties, which discourage infeasible or unsafe behavior. The

removed terms include torque-magnitude, DoF-velocity, DoF-acceleration, action-rate, torque-rate, and action-smoothness penalties, which can suppress aggressive but feasible actuation.

To avoid irregular actions without reintroducing conservative reward penalties, we regularize the policy mean with a second-difference smoothness loss. Let $\mu_\theta(o_t)$ denote the actor mean. We use

$$\mathcal{L}_{\text{GradCAPS}} = \frac{1}{2\sum_t g_t} \sum_t g_t \left\| \mu_\theta(o_{t+1}) - 2\mu_\theta(o_t) + \mu_\theta(o_{t-1}) \right\|_2^2, \tag{11}$$

where g_t masks out triplets that cross episode boundaries. The teacher is optimized with

$$\mathcal{L} = \mathcal{L}_{\text{PPO}} + \lambda_{\text{reg}} \mathcal{L}_{\text{GradCAPS}}. \tag{12}$$

This loss penalizes abrupt changes in action rate while still allowing large action changes when required by the reference motion.

Balance expert. For balance-critical residual motions, the main issue is early-training survivability. Under nominal gravity, an untrained policy often falls before it reaches informative tracking states. We therefore train the balance expert with a gravity continuation curriculum:

$$g_e = \alpha_e g_0, \qquad \alpha_e \in [\alpha_{\min}, 1], \tag{13}$$

where g_0 is nominal gravity and α_e gradually increases during training. Reduced gravity lengthens early rollouts and exposes useful contact, base-stabilization, and pose-tracking signal. Training then returns to nominal gravity, and all evaluation and deployment are performed under nominal dynamics.

Adaptive motion sampling. We keep adaptive motion sampling enabled throughout the pipeline, including teacher PPO training, DAgger student rollouts, and student RL fine-tuning. In each stage, the sampler assigns higher rollout probability to clips that currently produce larger tracking errors, while retaining a uniform sampling mixture to maintain coverage of the full dataset. Empirically, we found adaptive sampling to be a useful and sometimes necessary training component.

Adaptive sampling is also sensitive to implementation details. The version used in our experiments has small but critical differences from the samplers used in SONIC, EGM, and related systems, including how tracking errors are normalized, how temporal-bin difficulty is smoothed, how extreme scores are clipped, and how the resulting distribution is mixed with uniform sampling. Figure 3 shows the high-level procedure; the exact equations and hyperparameters are provided in App. A.2.

4.2 Motion-Routed Teacher Selection

After the two teacher-training rounds, we freeze the teacher bank Π_T and evaluate each teacher on every training clip using Eq. 7. For each motion τ_m, we select

$$k^*(m) = \arg \max_{k:\, \pi_T^k \in \Pi_T} \widehat{\text{SR}}(\pi_T^k, \tau_m), \tag{14}$$

which defines the fixed motion-level routing table

$$\tau_m \mapsto \pi_T^{k^*(m)}. \tag{15}$$

Because both capability experts are trained on the same residual set, routing does not rely on a manual dynamic/balance assignment. Instead, each motion is assigned to the frozen teacher that empirically tracks it best, and this assignment is used only to choose the supervision source during distillation.

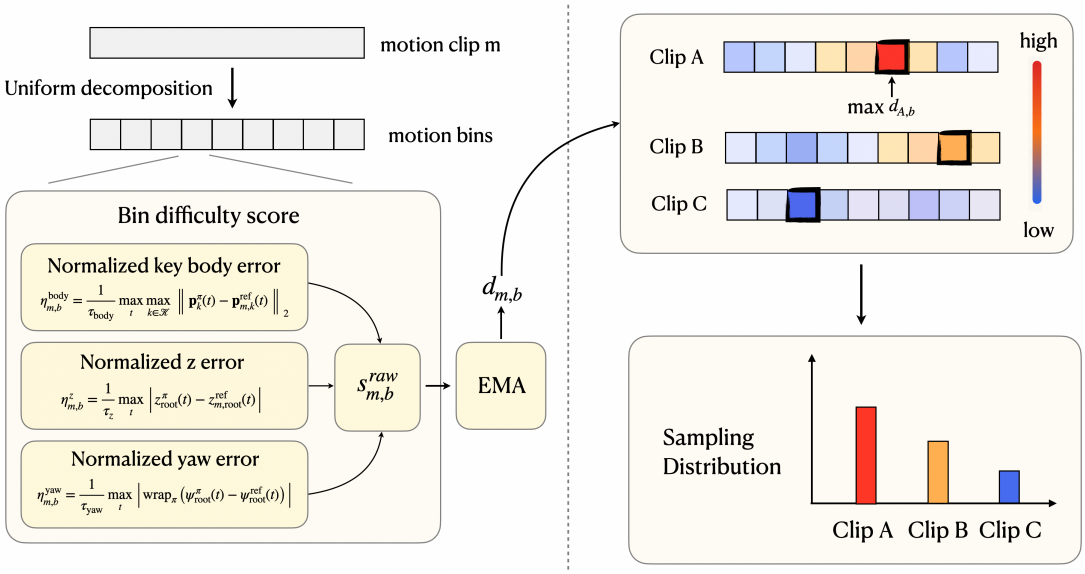

Figure 3: Adaptive motion sampling. Rollout tracking errors are converted into smoothed temporal-bin difficulty scores, reduced to clip-level difficulty scores, and then converted into clip sampling probabilities. Exact equations are given in App. A.2.

4.3 DAgger Distillation into a Single Student

We distill the routed teachers into a single student with DAgger-style behavior cloning. The student is rolled out in simulation using its own actions. For each visited state from motion τ_m, we query the routed teacher $\pi_T^{k^*(m)}$ using its privileged observation and train the student to match the teacher action mean with only deployable inputs.

The distillation objective is

$$\mathcal{L}_{\text{distill}} = \mathbb{E}\left[\left\|\mu_S(o_t^S) - \mu_T^{k^*(m)}(o_t^T)\right\|_2^2\right] + \lambda_{\text{aux}}\mathcal{L}_{\text{aux}}. \tag{16}$$

Here μ_S is the student action mean, $\mu_T^{k^*(m)}$ is the routed teacher action mean, and $\mathcal{L}_{\text{aux}}$ denotes the auxiliary representation losses used by the SONIC-Base student architecture when applicable. Thus, distillation transfers the behavior of the capability-aligned teachers while preserving the deployable observation interface and representation structure of the baseline controller.

4.4 RL Fine-tuning

The distilled student is finetuned with PPO under the deployable observation interface. Following the staged fine-tuning procedure in *Parkour in the Wild* [22], we initialize the actor from the DAgger-distilled student and use a small initial action standard deviation. Before updating the actor, we run a critic-only warm-up phase. During this phase, the actor is frozen and only the value function is trained. Rollouts are generated by the frozen actor, but Gaussian action noise is added to the actor output so that the critic observes a small neighborhood around the distilled policy rather than only deterministic student states.

After the critic warm-up, we gradually unfreeze the actor. Once the actor is fully unfrozen, we continue standard PPO fine-tuning with the deployable student observation and nominal environment dynamics. All teacher-related inputs and all training-only curriculum variables remain disabled throughout this stage.

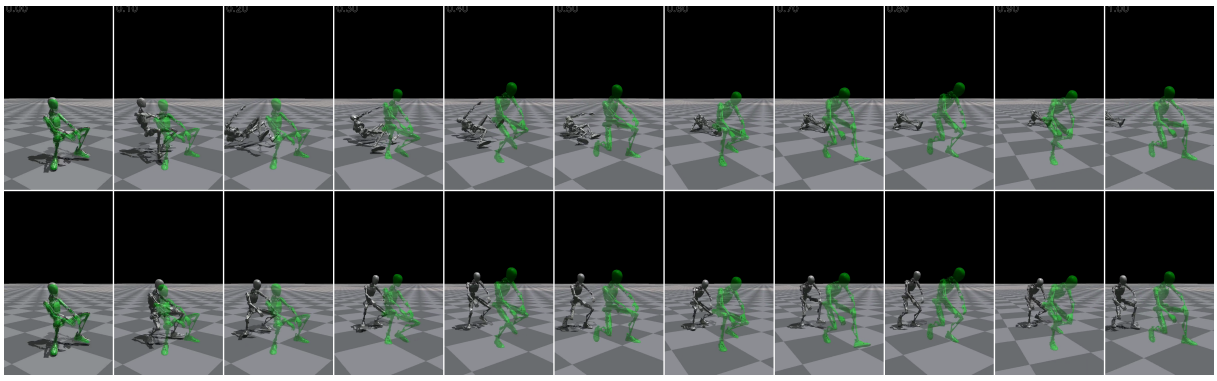

Figure 4: Qualitative case study: crouch-and-walk-forward motion. The upper strip shows the SONIC-Base and the lower strip shows the capability-aligned rollout. The green shadow indicates the reference motion when visible.

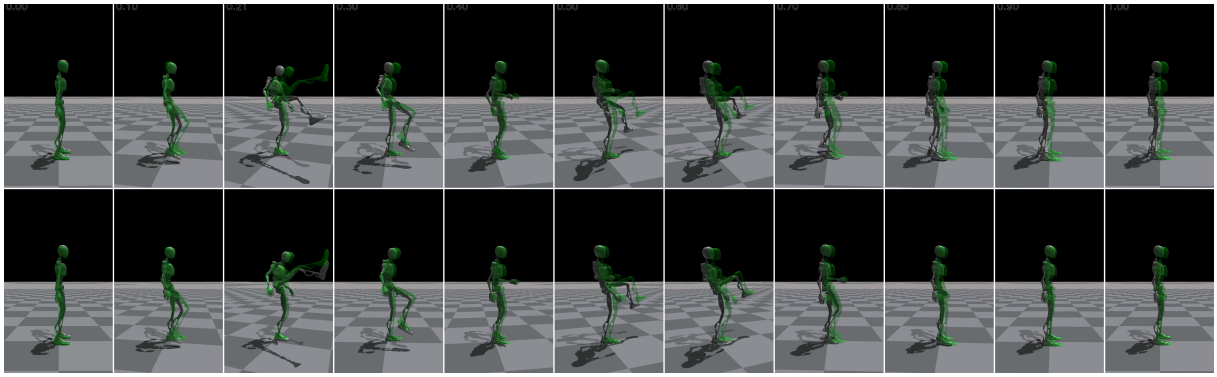

Figure 5: Qualitative case study: high-kick motion with a large single-leg swing. The upper strip shows the SONIC-Base and the lower strip shows the capability-aligned rollout.

5 Experiments

5.1 Experimental Setup

Embodiment. All experiments are conducted on a full-size 80 kg XPENG humanoid with planetary-roller-screw actuation and closed-chain mechanisms. This embodiment differs substantially from the Unitree G1 used in SONIC's released checkpoints. We therefore compare our method to the SONIC training recipe re-implemented on our platform, rather than to SONIC's released weights. Absolute numbers are not directly comparable to those reported in the SONIC paper. We acknowledge that our SONIC reimplementation may not fully match the performance of the released checkpoint on its native embodiment. Our claims are scoped to recipe-level comparison on the same hardware platform.

Training data. Our training set $\mathcal{D}_{\text{train}}$ is built from three open-source mocap datasets, AMASS [23], Bones-Seed [1], and BEAT [24], together with one curated mocap dataset. Based on the metadata duration sum, the curated mocap set contains 234 clips and 11.64 hours of motion; the AMASS subset contains 7,333 clips and 25.11 hours; the Bones-Seed subset contains 46,341 clips and 95.66 hours; and the BEAT subset contains 1,574 clips and 43.47 hours. In total, the training corpus contains 55,482 clips and 175.88 hours of motion.

Evaluation splits. We evaluate the proposed pipeline on the training set and two held-out evaluation sets. The IID held-out set, $\mathcal{D}_{\text{AMASS-eval}}$, is randomly sampled from AMASS and contains 10 hours of motion clips. It measures general tracking performance on unseen motions from the same broad data distribution.

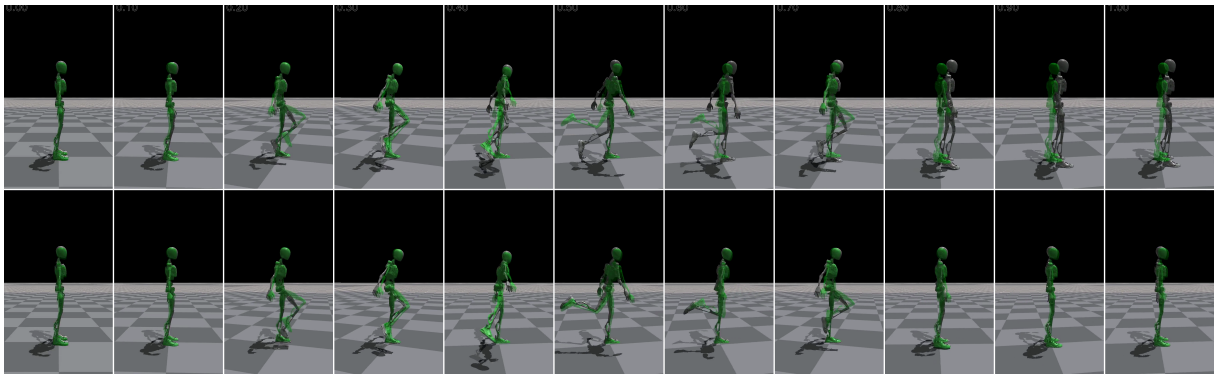

(a) Single-leg pose where the free leg is extended forward or folded backward.

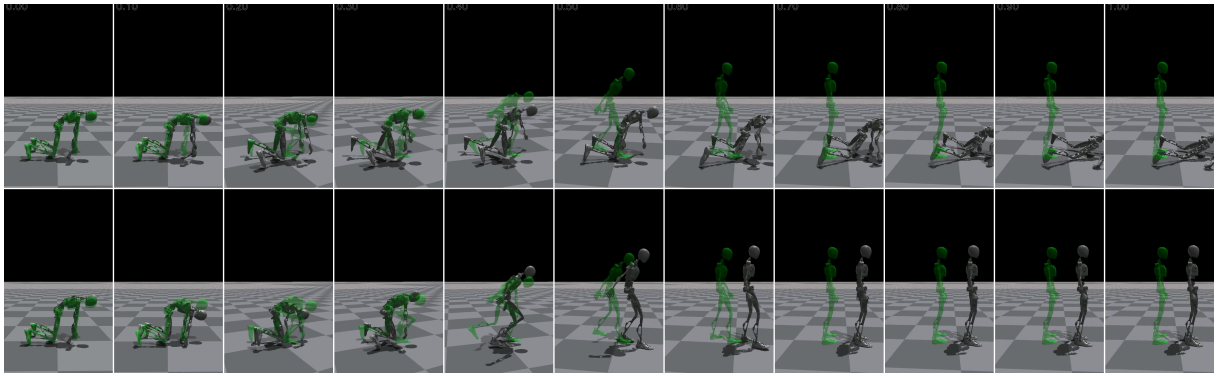

(b) Standing up from a knee-down pose.

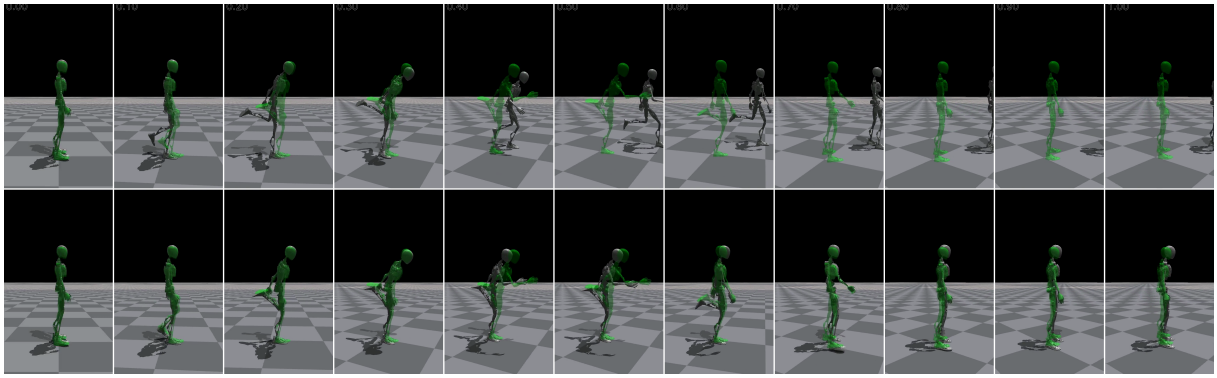

(c) One-leg stretching motion.

Figure 6: Qualitative case studies. In each case, the upper strip shows SONIC-Base and the lower strip shows the capability-aligned rollout.

The hard OOD held-out set, $\mathcal{D}_{\text{Omni-eval}}$, contains 227 curated mocap clips and approximately 3 hours of motion. It covers whole-body behaviors needed by a downstream manipulation policy, including locomotion in different directions and speeds, turning, bending, squatting, reaching, and object-pickup motions. Compared with random AMASS clips, this set contains a higher concentration of capability-demanding motions and is therefore used as a hard-motion stress test.

We additionally report diagnostic results on two long-tail training subsets: $\mathcal{D}_{\text{dynamic}}$ and $\mathcal{D}_{\text{balance}}$. $\mathcal{D}_{\text{dynamic}}$ contains high-dynamic motions such as fast running, jumping, rapid direction changes, and aggressive contact transitions. $\mathcal{D}_{\text{balance}}$ contains balance-critical motions such as single-support poses, hand-supported poses, push-up-like motions, and hands-down feet-up motions.

Training setup. All policies are trained in our reimplementation of the SONIC algorithm. Unless otherwise stated, RL training uses 8 GPUs with 2,048 parallel environments per GPU, for a total of 16,384 environments. The main non-finetuned checkpoints are trained for 40k iterations. This budget is used for the SONIC-Base, the no-smoothness baseline, and the capability-aligned teachers, so their training-set recovery results are compared under the same iteration budget. RL fine-tuning is a separate final stage initialized from the distilled multi-teacher student.

Failure mining. We mine the residual set $\mathcal{R}_{\text{gen}}$ by evaluating the trained general teacher with Eq. 7 and selecting clips satisfying $\widehat{\text{SR}}(\pi_T^{\text{gen}}, \tau_m) < \rho_{\text{fail}}$, as defined in Eq. 8. The mined set is fixed before expert training and is shared by both capability experts; motion-specific teacher selection is deferred to the rollout-based routing stage.

Compared methods. We compare the following policies:

- **SONIC-Base**: the reference WBC pipeline with reward-level effort and temporal-control regularization.
- **No-smoothness baseline**: a tracking-focused policy that removes effort and temporal-control reward penalties. This baseline tests whether conservative reward regularization creates a real capability bottleneck, but it is not considered deployable because it produces high-frequency, non-smooth actions.
- **Single-teacher student**: a single student distilled from one general privileged teacher.
- **Multi-teacher student**: a single student distilled from the routed general, dynamic, and balance teachers.
- **Multi-teacher student + RL fine-tuning**: the final policy, initialized from the multi-teacher distilled student and finetuned with PPO.

Adaptive motion sampling is enabled throughout teacher training, DAgger distillation rollouts, and RL fine-tuning. We found it to be a useful but sensitive training component. The exact sampler used in our experiments differs in small but critical ways from SONIC-/EGM-style variants; details are provided in App. A.2.

5.2 Evaluation Protocol and Metrics

All final policies are evaluated using the deployable observation interface. Privileged teacher observations, reduced-gravity curriculum variables, teacher identifiers, and routing information are disabled at evaluation time. The actor is evaluated deterministically using its action mean. Each reference clip is rolled out from its initial reference state for the full reference horizon or until a termination event occurs.

All reported values are averaged over three training seeds. For each method and seed, each clip is evaluated with $R = 5$ rollouts under the standard domain randomization setting. Tables report clip-uniform averages. Success-rate improvements are reported in percentage points.

Success rate. Success rate (SR) follows the standard threshold-based tracking rule used in humanoid WBC evaluation. A rollout is counted as successful if, for the entire clip, its root-height error, root-yaw error, and maximum key-body position error remain below fixed thresholds:

$$\delta_z^0 = 0.20\ \text{m}, \qquad \delta_{\text{yaw}}^0 = 0.50\ \text{rad}, \qquad \delta_{\text{kb}}^0 = 0.50\ \text{m}. \tag{17}$$

The threshold checks use zero-frame windows, so any frame exceeding one of the thresholds marks the rollout as failed.

Threshold-robust success. To reduce dependence on a single threshold choice, we additionally report the Success–Tolerance Curve (STC) and Threshold-Integrated Success (TIS). STC recomputes SR after scaling all default thresholds by a factor $s \geq 0$:

$$\delta_z(s) = s\delta_z^0, \qquad \delta_{\text{yaw}}(s) = s\delta_{\text{yaw}}^0, \qquad \delta_{\text{kb}}(s) = s\delta_{\text{kb}}^0. \tag{18}$$

Thus, $s = 1$ gives the default SR, $s < 1$ gives stricter thresholds, and $s > 1$ gives looser thresholds. TIS summarizes the curve as

$$\text{TIS}(\pi; \mathcal{D}) = \int_0^\infty \text{SR}_\pi(s; \mathcal{D}) \frac{ds}{(1+s)^2}. \tag{19}$$

TIS is bounded in $[0, 1]$ and avoids choosing a maximum threshold scale. We use SR for comparability with prior work and TIS to expose robustness across tracking tolerances.

Tracking and smoothness metrics. We report MPJPE in millimeters. MPJPE is the mean Euclidean Cartesian tracking error over evaluated joints or key bodies. We also report Motion-Salience Weighted MPJPE (MPJPE-W) on long-tail subsets. MPJPE-W weights each joint or key body according to its normalized cumulative motion in the heading-local root frame, emphasizing the body parts that define a given reference clip. Figure 7 illustrates the intuition behind MPJPE-W and STC: MPJPE-W highlights motion-salient body parts, while STC exposes how policy rankings can change as the success tolerance is varied. Formal details are given in App. A.3.

For control smoothness, we report action rate:

$$R_a = \frac{1}{T-1} \sum_{t=1}^{T-1} \|a_{t+1} - a_t\|_2^2. \tag{20}$$

Lower action rate indicates smoother actions and is used as a deployment-quality diagnostic.

5.3 Main Results

Q1: Does the final policy improve held-out tracking while preserving control quality? Table 3 reports held-out tracking and action smoothness. The no-smoothness baseline is included as a diagnostic rather than a deployable policy. Removing effort and temporal-control reward penalties improves single-threshold SR, confirming that conservative reward regularization creates a real capability bottleneck. However, this comes at the cost of much higher action rate. The goal of the proposed pipeline is therefore not merely to maximize default-threshold SR, but to recover the tracking benefit of less conservative acquisition while improving threshold-integrated tracking, Cartesian tracking error, motion-salience-aware tracking, and deployable control quality through auxiliary policy regularization, routed distillation, and RL fine-tuning.

Compared with SONIC-Base, the RL-finetuned policy improves AMASS SR from 98.18% to 99.26% and Omni SR from 91.81% to 94.89%. It also gives the best TIS on both held-out sets, improving AMASS TIS from 0.7631 to 0.8034 and Omni TIS from 0.7123 to 0.7449. The same trend appears in tracking error: AMASS MPJPE decreases from 68.26 ± 18.42 mm to 63.63 ± 18.91 mm, AMASS MPJPE-W

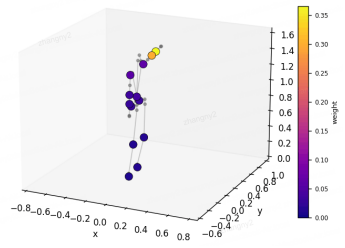

(a) Fast left-hand waving

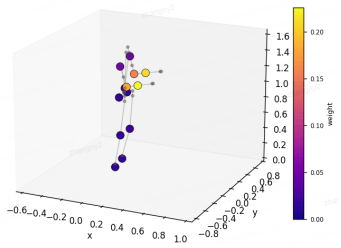

(b) Two-hand object holding

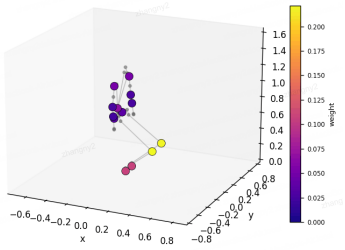

(c) Squat-and-recover motion

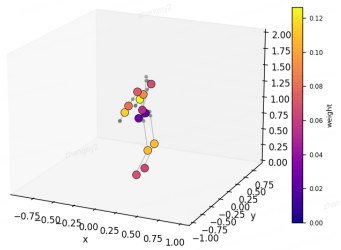

(d) Vertical jump

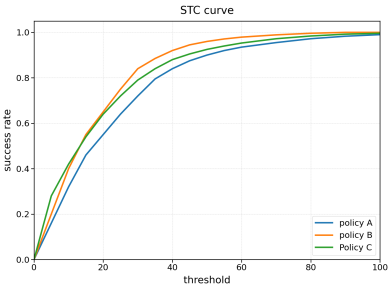

(e) Success–Tolerance Curve

Figure 7: MPJPE-W and STC as complementary evaluation tools for tracking WBC. Left: Motion-Salience Weighted MPJPE assigns higher importance to body parts that are more active in the reference motion, exposing motion-specific tracking quality that uniform MPJPE can obscure. Right: Success–Tolerance Curve visualizes success rate as a function of tolerance, revealing threshold sensitivity and policy trade-offs that are hidden by a single scalar success rate.

Table 3: Held-out tracking and control quality. SR is reported in percent. MPJPE and MPJPE-W are reported in millimeters as mean $\pm$ one standard deviation, where $\pm$ denotes a 1σ error bar. TIS denotes Threshold-Integrated Success. Action Rate measures action smoothness on held-out rollouts. Higher SR and TIS are better; lower MPJPE, MPJPE-W, and Action Rate are better.

Method	$\mathcal{D}_{\text{AMASS-eval}}$				$\mathcal{D}_{\text{Omni-eval}}$				Smoothness
	SR% ↑	TIS ↑	MPJPE ↓	MPJPE-W ↓	SR% ↑	TIS ↑	MPJPE ↓	MPJPE-W ↓	Action Rate ↓
SONIC-Base	98.18	0.7631	68.26 ± 18.42	84.92 ± 39.04	91.81	0.7123	70.39 ± 23.00	79.72 ± 38.47	**0.54**
No-smoothness baseline	**99.46**	0.7806	66.18 ± 15.92	81.82 ± 37.21	**95.33**	0.7293	66.73 ± 15.13	75.39 ± 32.99	1.46
Single-teacher student	98.75	0.7795	65.95 ± 22.08	81.82 ± 40.47	94.63	0.7374	68.44 ± 33.63	76.78 ± 44.58	0.56
Multi-teacher student	99.02	0.7876	64.05 ± 20.26	78.95 ± 38.44	92.95	0.7421	67.56 ± 31.59	75.80 ± 44.90	0.66
RL fine-tuning	99.26	**0.8034**	$\mathbf{63.63 \pm 18.91}$	$\mathbf{78.26 \pm 38.13}$	94.89	**0.7449**	$\mathbf{65.11 \pm 19.38}$	$\mathbf{72.65 \pm 34.99}$	1.03

decreases from 84.92 ± 39.04 mm to 78.26 ± 38.13 mm, Omni MPJPE decreases from 70.39 ± 23.00 mm to 65.11 ± 19.38 mm, and Omni MPJPE-W decreases from 79.72 ± 38.47 mm to 72.65 ± 34.99 mm.

The no-smoothness baseline confirms the capability bottleneck most directly. It achieves the highest default-threshold SR on both AMASS-eval and Omni-eval, with 99.46% and 95.33%, respectively. This shows that removing conservative effort and temporal-control rewards can make held-out motions easier to track. However, its Action Rate increases from 0.54 for SONIC-Base to 1.46, making it unsuitable as a deployable controller. The RL-finetuned policy does not dominate the no-smoothness baseline in default SR, but it achieves better TIS, lower MPJPE, lower MPJPE-W, and a substantially lower Action Rate of 1.03. Thus, the final policy recovers much of the tracking benefit exposed by no-smoothness training while avoiding its non-deployable high-frequency behavior.

The student rows show the role of distillation and fine-tuning. The single-teacher and multi-teacher students already improve most tracking-error metrics over SONIC-Base while keeping action rate close to the regularized baseline. RL fine-tuning then improves the threshold-integrated and Cartesian tracking metrics further, producing the best TIS, MPJPE, and MPJPE-W on both held-out sets. We therefore interpret RL fine-tuning as a generalization and deployment-quality stage: it does not simply optimize the default success threshold, but improves the broader tolerance spectrum and the accuracy of the tracked

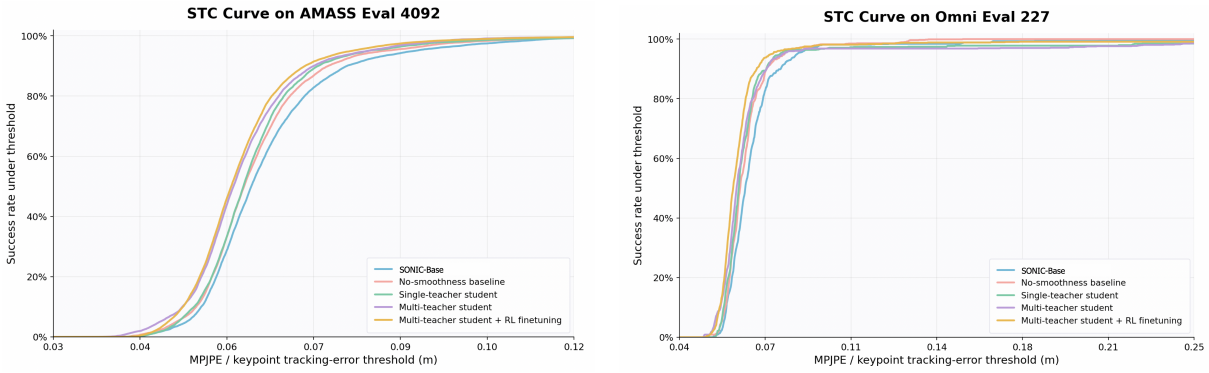

(a) AMASS-eval (b) Omni-eval

Figure 8: Key-body-tolerance Success–Tolerance Curves on the two held-out evaluation sets. Unlike the full STC definition, which jointly scales the root-height, root-yaw, and key-body tracking thresholds, this figure sweeps only the allowed key-body tracking-error tolerance and reports the resulting success rate. Curves that are shifted left or upward indicate that a policy succeeds under stricter key-body error tolerances, whereas saturation at loose tolerances can hide differences that are visible in the stricter regime.

Table 4: Long-tail training-set recovery. We report SR and MPJPE on the full training set and two diagnostic long-tail subsets. For the diagnostic subsets, we additionally report MPJPE-W. MPJPE and MPJPE-W values are reported as mean $\pm 1\sigma$ error bars in millimeters, and SR is reported in percent. All non-finetuned checkpoints use the same 40k training budget.

Method	Full Train		$\mathcal{D}_{\text{dynamic}}$			$\mathcal{D}_{\text{balance}}$		
	MPJPE ↓	SR (%) ↑	MPJPE ↓	MPJPE-W ↓	SR (%) ↑	MPJPE ↓	MPJPE-W ↓	SR (%) ↑
SONIC-Base	72.36 ± 30.98	98.48	80.17 ± 29.52	87.05 ± 40.99	96.41	86.66 ± 67.44	101.99 ± 73.06	90.60
No-smoothness baseline	$\mathbf{67.74 \pm 18.82}$	99.21	75.77 ± 25.17	81.98 ± 37.40	**98.75**	80.99 ± 60.09	95.01 ± 65.63	93.61
Dynamic expert, Grad-CAPS	68.90 ± 29.84	99.13	$\mathbf{75.64 \pm 27.06}$	$\mathbf{81.58 \pm 37.46}$	98.35	79.20 ± 61.58	93.09 ± 67.43	93.55
Balance expert, gravity curriculum	68.70 ± 32.69	**99.22**	75.96 ± 26.93	81.62 ± 36.11	97.77	76.32 ± 49.88	90.22 ± 55.64	92.99
Multi-teacher student	68.27 ± 28.51	98.76	76.93 ± 31.19	82.94 ± 39.20	97.77	$\mathbf{75.36 \pm 44.47}$	$\mathbf{88.61 \pm 50.54}$	**94.73**
RL fine-tuning	68.89 ± 28.45	98.69	77.28 ± 29.59	83.39 ± 37.96	97.92	79.86 ± 59.40	93.41 ± 64.88	92.55

motion.

Figure 8 further visualizes the held-out results using Success–Tolerance Curves. Instead of evaluating each policy at one fixed success threshold, the curves sweep the allowed keypoint tracking-error tolerance and report the fraction of successful rollouts at each tolerance. The curves explain why the scalar SR alone is incomplete in this regime. On both AMASS-eval and Omni-eval, the no-smoothness baseline achieves the highest default-threshold SR, but it is not uniformly preferable once the full tolerance spectrum and action smoothness are considered. The RL-finetuned policy achieves the best TIS and the lowest MPJPE/MPJPE-W, indicating stronger integrated tracking performance across tolerances even when its default SR is slightly below the no-smoothness baseline.

The STC curves also reveal threshold sensitivity and curve crossings that a single SR value cannot show. Several policies approach saturation under loose tolerances, where their differences become visually small. Under stricter and medium tolerances, however, the policies separate more clearly, exposing whether a method improves precise tracking or only succeeds after the threshold is relaxed. This is why we report SR together with TIS and tracking-error metrics: default SR preserves comparability with prior work, while STC and TIS show whether the improvement is robust across the tolerance spectrum.

5.4 Long-Tail Recovery Analysis

Q2: Are long-tail training motions recovered by capability-aligned training rather than by exposure alone? Table 4 evaluates whether strong average training-set performance hides weaknesses on structured long-tail motion regimes. SONIC-Base already performs well on the full training set,

achieving 98.48% SR and 72.36 ± 30.98 mm MPJPE. However, its performance is lower on the diagnostic subsets, especially on balance-critical motions, where SR drops to 90.60% and MPJPE-W increases to 101.99 ± 73.06 mm. This gap shows that aggregate training-set metrics can obscure systematic failures on hard motion regimes.

The no-smoothness baseline exposes a capability bottleneck. Removing effort and temporal-control reward penalties improves full-training MPJPE to 67.74 ± 18.82 mm and increases full-training SR to 99.21%. It also achieves the highest dynamic-subset SR, 98.75%, while improving both dynamic and balance tracking errors relative to SONIC-Base. These results indicate that conservative reward regularization can suppress learnable long-tail behavior, especially for high-dynamic motions. However, as shown in Table 3, this policy has a much higher action rate and is therefore not a deployable solution. Thus, no-smoothness training is useful as a diagnostic, but not as the final controller.

The capability-aligned experts recover different parts of the long tail under the same 40k training budget. The Grad-CAPS dynamic expert achieves the lowest dynamic-subset errors, reducing MPJPE to 75.64 ± 27.06 mm and MPJPE-W to 81.58 ± 37.46 mm, while maintaining a high dynamic SR of 98.35%. In contrast, the gravity-curriculum balance expert improves balance-critical tracking more strongly, reducing balance MPJPE from 86.66 ± 67.44 mm to 76.32 ± 49.88 mm and MPJPE-W from 101.99 ± 73.06 mm to 90.22 ± 55.64 mm. This specialization pattern suggests that the two expert recipes do more than repeatedly expose the policy to difficult motions: they bias learning toward different useful operating regimes.

The multi-teacher student consolidates these complementary capabilities into a single student policy. Although it does not outperform the dynamic expert on dynamic-subset error, it achieves the strongest balance-subset performance, with the highest balance SR of 94.73% and the lowest balance errors: 75.36 ± 44.47 mm MPJPE and 88.61 ± 50.54 mm MPJPE-W. It also preserves strong full-training performance, with 98.76% SR and 68.27 ± 28.51 mm MPJPE. These results support the role of motion-routed distillation: the dynamic and balance teachers provide complementary coverage, and the student combines their behaviors into one policy with deployable observations.

The RL-finetuned policy should not be interpreted as the main source of training-set long-tail recovery. Compared with the multi-teacher student, it does not improve the full-training or diagnostic-subset metrics: balance SR decreases from 94.73% to 92.55%, and balance MPJPE-W increases from 88.61 ± 50.54 mm to 93.41 ± 64.88 mm. Its role is instead clarified by Table 3: RL fine-tuning is used as the final generalization and deployment-quality stage, while the main evidence for Q2 comes from capability-aligned expert acquisition and multi-teacher distillation.

5.5 Smoothness Analysis

Q3: Which components determine the tracking–smoothness trade-off? We answer this question with an aggregate smoothness-placement ablation and a frequency-domain jitter diagnosis. The goal is to distinguish two effects that are often conflated by reward design: whether a controller can acquire high-dynamic tracking behavior, and whether the resulting action sequence is smooth enough for deployment.

Setup. We ablate where smoothness is imposed in the policy-learning pipeline. The reward-smooth baseline keeps temporal and effort penalties in the RL reward. NoSmooth removes these penalties and serves as a tracking-first reference. CAPS and Grad-CAPS also remove reward-level smoothness penalties, but add auxiliary policy losses during optimization. All variants use the same tracking rewards, training data, and evaluation protocol.

Aggregate trade-off. Table 5 shows that removing reward-level smoothness penalties improves held-out tracking success but substantially increases action variation. NoSmooth improves AMASS-eval SR from 98.18% to 99.46% and Omni-eval SR from 91.81% to 95.33%. It also improves AMASS TIS from 0.7631 to 0.7806 and Omni TIS from 0.7123 to 0.7293. However, this tracking gain comes with a large smoothness cost: Action Rate increases from 0.5447 to 1.4634, and Action Jerk increases from 0.4905 to 2.0091. This confirms that reward-level smoothness penalties are conservative for tracking, but that tracking-only optimization does not by itself produce deployable control.

Table 5: Smoothness-placement ablation on held-out evaluation sets. SR is reported in percent. TIS denotes Threshold-Integrated Success. MPJPE and MPJPE-W are both reported in millimeters as mean $\pm 1\sigma$ error bars. Action Rate and Action Jerk measure action smoothness on held-out rollouts. Higher SR and TIS are better; lower MPJPE, MPJPE-W, Action Rate, and Action Jerk are better.

Variant	Smoothness mechanism	$\mathcal{D}_{\text{AMASS-eval}}$				$\mathcal{D}_{\text{Omni-eval}}$				Smoothness	
		SR% ↑	TIS ↑	MPJPE ↓	MPJPE-W ↓	SR% ↑	TIS ↑	MPJPE ↓	MPJPE-W ↓	Action Rate ↓	Action Jerk ↓
SONIC-Base	reward penalty	98.18	0.7631	68.26 ± 18.42	84.92 ± 39.04	91.81	0.7123	70.39 ± 23.00	79.72 ± 38.47	**0.5447**	**0.4905**
No-smoothness baseline	none	**99.46**	**0.7806**	66.18 ± 15.92	81.82 ± 37.21	**95.33**	0.7293	66.73 ± 15.13	75.39 ± 32.99	1.4634	2.0091
Dynamic expert, CAPS	auxiliary temporal loss	98.75	0.7762	$\mathbf{65.22 \pm 27.70}$	$\mathbf{80.40 \pm 43.80}$	93.30	0.7208	$\mathbf{66.56 \pm 31.04}$	$\mathbf{75.13 \pm 44.08}$	0.8463	0.8326
Dynamic expert, Grad-CAPS	auxiliary gradient-temporal loss	98.95	0.7762	66.59 ± 22.31	82.24 ± 40.23	93.39	**0.7351**	69.17 ± 34.22	77.65 ± 47.52	0.5627	0.5117

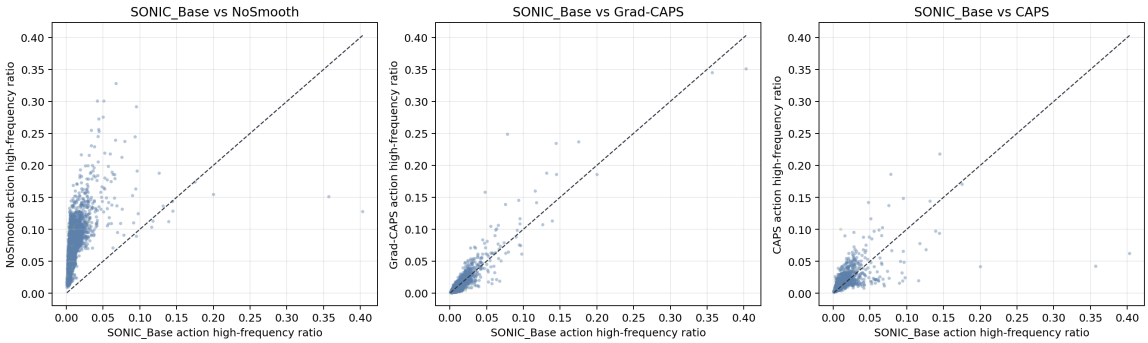

Figure 9: Clip-level high-frequency action-energy comparison against SONIC-Base. Each point is one clip. The x-axis is the high-frequency action-energy ratio of SONIC-Base, and the y-axis is the ratio of another variant on the same clip. Points above the diagonal are less smooth than SONIC-Base on that clip, while points below the diagonal are smoother. NoSmooth moves almost all clips above the diagonal, showing that disabling reward-level smoothness creates a distribution-wide jitter increase rather than a few outliers. Grad-CAPS shifts most clips below the diagonal, indicating broad high-frequency suppression; CAPS reduces jitter relative to NoSmooth but is less consistently below SONIC-Base.

Auxiliary policy losses recover different operating points on this tracking–smoothness trade-off. CAPS gives the best Cartesian tracking errors in this ablation, reducing AMASS MPJPE from 68.26 ± 18.42 mm to 65.22 ± 27.70 mm and Omni MPJPE from 70.39 ± 23.00 mm to 66.56 ± 31.04 mm. It also gives the lowest MPJPE-W on both held-out sets: 80.40 ± 43.80 mm on AMASS-eval and 75.13 ± 44.08 mm on Omni-eval. However, CAPS only partially recovers smoothness, with Action Rate 0.8463 and Action Jerk 0.8326.

Grad-CAPS provides the strongest smoothness recovery among the tracking-focused variants. Its Action Rate is 0.5627 and its Action Jerk is 0.5117, close to the reward-smooth SONIC-Base values of 0.5447 and 0.4905, while still improving over SONIC-Base in MPJPE and MPJPE-W on both held-out sets. Grad-CAPS also obtains the best Omni-eval TIS in this ablation, 0.7351. Thus, at the tested coefficients, CAPS is the most tracking-error-favorable auxiliary loss, whereas Grad-CAPS is the most smoothness-favorable auxiliary loss while still preserving much of the tracking gain from removing reward-level smoothness penalties.

Distribution-level jitter. Figure 9 shows that the smoothness degradation of NoSmooth is not confined to a small number of difficult motions. Across 4319 evaluated clips, NoSmooth has higher high-frequency action energy than SONIC-Base on 4309 clips. In contrast, Grad-CAPS is below SONIC-Base on 3441 clips, indicating that its smoothing effect is distribution-wide rather than case-specific. CAPS also reduces the large NoSmooth jitter increase, but only 584 clips fall below the SONIC-Base diagonal, suggesting that CAPS is a weaker high-frequency suppressor at the tested coefficient. This agrees with Table 5: CAPS improves tracking errors most, while Grad-CAPS more consistently suppresses high-frequency action variation.

Frequency content. Figure 10 explains what the increased Action Rate and Action Jerk in Table 5 consist of. We compute the action power spectrum for each episode by applying FFT to the de-meaned action

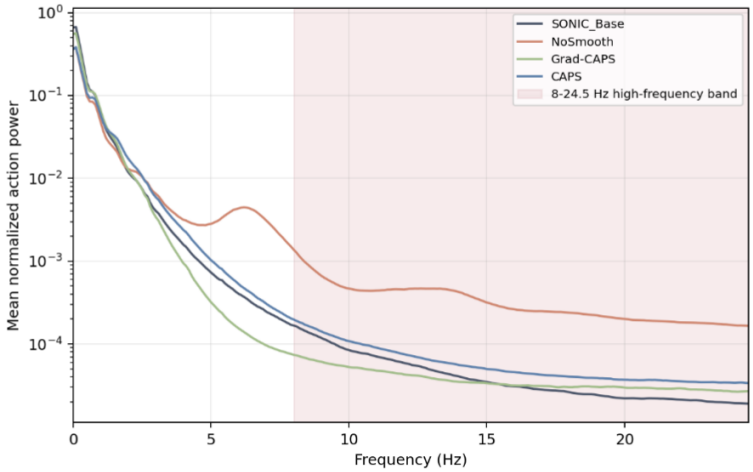

Figure 10: Mean normalized action power spectral density under different smoothness placements. The x-axis is frequency and the y-axis is normalized action power, i.e., the relative distribution of action-variation energy across frequencies rather than the absolute action magnitude. The shaded region marks the high-frequency jitter band. A larger curve in this band means that a larger fraction of action variation is concentrated in rapid action oscillations. NoSmooth has a much larger high-frequency component, whereas CAPS and Grad-CAPS suppress this component close to the reward-smooth baseline.

trajectories and summing the spectral power over action dimensions. The spectrum is then normalized by the total action power in the 0.5–25 Hz band and averaged across valid episodes. Therefore, the plotted mean normalized action power is a dimensionless relative spectral density: it reflects how action variation is distributed over frequency, rather than the absolute action magnitude. Higher values in the 8–25 Hz band indicate that more action energy is concentrated in high-frequency oscillations, which corresponds to stronger action jitter.

NoSmooth does not only use larger low-frequency actions to track dynamic motions; it introduces a clear high-frequency action component. Its action high-frequency ratio is 0.063, compared with 0.009 for SONIC-Base. CAPS reduces this ratio to 0.011, and Grad-CAPS further reduces it to 0.007. Thus, the extra action variation under NoSmooth corresponds to high-frequency control jitter, while the auxiliary losses suppress the frequency band that is most relevant to deployment smoothness.

Time-domain behavior. Figure 11 shows how the spectral difference appears in an actual high-dynamic rollout. On this successful backward-running clip, NoSmooth has the largest action-rate and action-jerk means (4.571 and 6.633), compared with SONIC-Base (1.771 and 2.147). CAPS reduces them to 2.507 and 3.089, while Grad-CAPS further reduces them to 1.319 and 1.341. The raw action trace shows the same pattern: removing smoothness introduces rapid zig-zag updates, whereas auxiliary policy losses suppress these oscillations while preserving successful tracking on the clip.

Together, Figs. 9–11 support the smoothness-placement interpretation suggested by Table 5. Reward-level penalties help suppress high-frequency control artifacts but can limit tracking performance. Removing them improves default-threshold SR and TIS, but exposes distribution-wide high-frequency jitter. Auxiliary policy losses provide a separate knob for choosing the operating point on this trade-off: CAPS gives the best MPJPE and MPJPE-W in the aggregate table, whereas Grad-CAPS gives stronger high-frequency suppression in the clip-level scatter, the spectrum, and the representative time-domain rollout.

5.6 Ablations

Teacher observation design. We also test whether privileged teacher observations matter for downstream student quality. The student observation is fixed across this ablation; only the teacher observation changes.

The Omni-style privileged teacher observation improves teacher acquisition and produces cleaner action

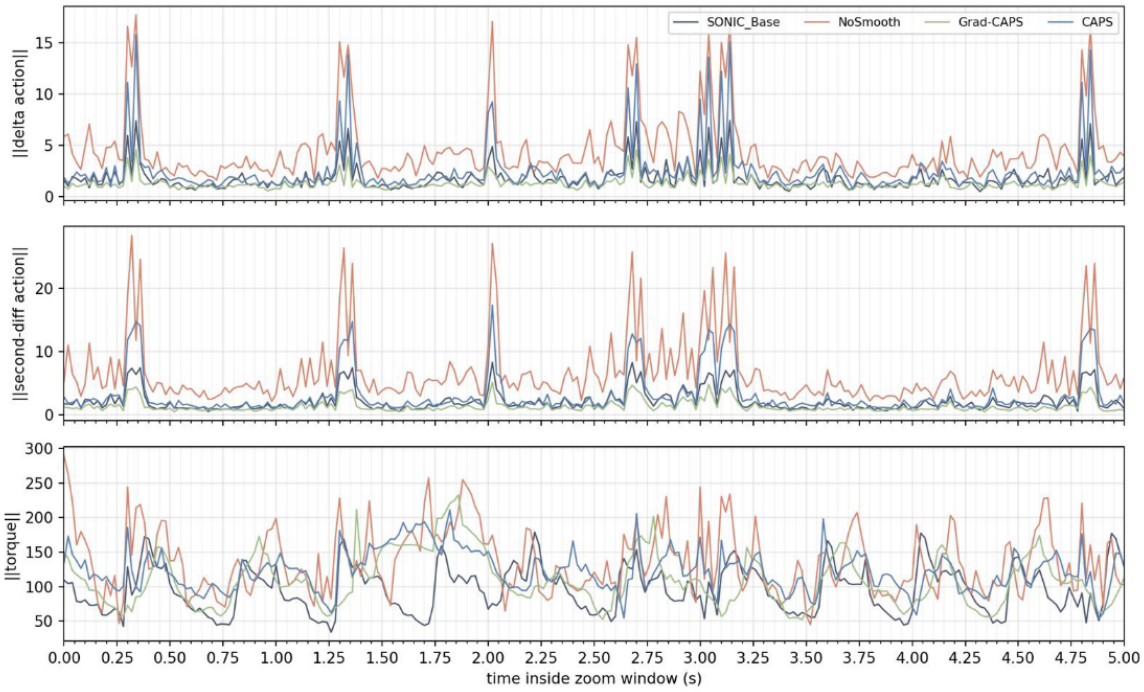

Figure 11: Representative successful high-dynamic backward-running clip. The rows show an oscillatory action dimension, the action-rate norm, the action-jerk norm, and the torque norm over a 5 s window. Since all variants successfully track this clip, the comparison isolates smoothness under successful behavior rather than failure artifacts. NoSmooth produces visibly larger action-rate and action-jerk spikes, while CAPS and especially Grad-CAPS reduce these oscillations.

Table 6: Teacher observation ablation. The student always receives the same robot-available observation; only the privileged teacher observation changes. SR is reported in percent and MPJPE is reported in millimeters.

Teacher observation	$\mathcal{D}_{\text{AMASS-eval}}$		$\mathcal{D}_{\text{Omni-eval}}$	
	SR (%) ↑	MPJPE ↓	SR (%) ↑	MPJPE ↓
Motion-privileged + proprioception	95.31	67.12	87.75	**74.13**
Omni-privileged + motion-privileged + proprioception	**96.20**	**65.97**	**87.84**	76.97

labels during distillation. Because the student does not receive these privileged variables, the improvement indicates better supervision rather than a larger deployment-time observation space.

5.7 Qualitative Results

Q4: What failure modes are corrected by capability-aligned experts? Figures 4–6c show five representative long-tail case studies. Each figure uses the full page width to make the temporal motion strip readable. Across these cases, the SONIC-Base often tracks the easy portions of the clip but fails during low-support, large-leg-motion, or recovery phases. The capability-aligned rollouts maintain support for longer and track the reference more closely through the critical transition.

6 Limitations

Although the proposed pipeline improves long-tail humanoid whole-body control, it does not fully solve the long-tail coverage problem. Training-set coverage is improved but remains below complete coverage. One difficulty is that failure attribution is still coupled with reference quality and motion feasibility:

some residual failures may come from imperfect retargeted references, data artifacts, or motions near the physical limits of the embodiment. However, we also observe clips that appear learnable but are still not reliably acquired even by the privileged teacher, suggesting that unresolved acquisition failures remain beyond reference-quality issues alone. In addition, RL fine-tuning introduces a trade-off that is not yet fully understood: in some settings, it reduces training-set coverage while improving held-out evaluation metrics. Understanding this coverage–generalization trade-off is an important direction for future work.

We also observe residual motion-quality artifacts in the final checkpoints. In particular, after removing reward-level effort and temporal-control regularization, some clips still exhibit low-frequency sway. This artifact is qualitatively different from high-frequency action chatter. CAPS and Grad-CAPS penalize local temporal variation in consecutive actions or action differences, but a slow periodic sway can have small per-step action changes and therefore may not be strongly penalized by these objectives. Our experiments are consistent with this interpretation: increasing the CAPS or Grad-CAPS loss weight does not eliminate the low-frequency sway. This suggests that additional mechanisms may be required, such as reference correction, phase-level stabilization, frequency-domain regularization, controller-level damping, or improved state/action representations. Due to time and resource constraints, we leave a systematic study of this phenomenon to future work.

A further limitation is the complexity of the pipeline. The full method requires residual failure mining, multiple privileged teacher-training stages, rollout-based teacher routing, DAgger-style distillation, and post-distillation RL fine-tuning. This makes the system substantially heavier and longer than a single-policy training recipe. Each stage also introduces additional implementation choices and hyperparameters, including failure thresholds, sampling distributions, routing criteria, auxiliary loss weights, and fine-tuning schedules. Reducing this engineering cost, or integrating capability alignment into a simpler unified training procedure, remains an important practical direction.

Our experiments are also limited by compute and training time. All comparisons in this work, including the baseline, general teacher training, capability-aligned expert training, DAgger distillation, and RL fine-tuning, were conducted under a relatively small compute budget. The current results therefore provide evidence that the proposed pipeline is effective in a resource-constrained regime, but they do not establish its behavior under saturated training. Further experiments with larger compute budgets, larger motion datasets, and more converged optimization are needed to determine whether the same gains persist at greater scale.

Finally, our real-robot validation is still limited. Although real-robot evaluation is a common challenge in humanoid WBC, the current paper does not yet include systematic quantitative deployment results. Moreover, our experiments are conducted on a new robot platform that is still under development and has not yet been publicly released. Real-robot deployment is in progress on an internal XPENG humanoid platform. We will defer deployment demonstrations and systematic quantitative real-robot evaluation in a future version after the platform is publicly released.

7 Conclusion

We studied humanoid motion-tracking WBC in the high-coverage regime, where the remaining failures are not only held-out generalization errors but also residual training-set failures. Our results show that these failures are concentrated in high-dynamic and balance-critical regimes, and that they are not fully explained by insufficient exposure alone. Conservative effort and temporal-control rewards can suppress aggressive but feasible tracking behavior, while nominal-gravity training can prevent balance-critical clips from producing useful early learning signal.

We proposed *Athena-WBC*, a compact teacher-student pipeline that adapts the acquisition recipe to the capability required by the residual motions. Dynamic experts retain tracking and physical-constraint terms while moving smoothness pressure from the reward into auxiliary policy regularization. Balance experts use a gravity curriculum to improve early-training survivability. Motion-routed DAgger distillation then compresses the complementary teachers into one student, and RL fine-tuning improves held-out

tracking and deployment quality. This separates two roles: multi-teacher distillation provides the strongest training-set long-tail recovery, while RL fine-tuning produces the final controller used for evaluation and hardware deployment.

Beyond the training pipeline, we introduced evaluation tools intended for high-coverage WBC. A single threshold-based success rate is often insufficient when policies are already strong, because small threshold changes can alter rankings and hide whether gains occur under strict or loose tolerances. Success–Tolerance Curves expose this behavior by sweeping the tracking tolerance, and Threshold-Integrated Success provides a scalar summary without choosing an arbitrary maximum tolerance. We also proposed Motion-Salience Weighted MPJPE, which emphasizes the joints and key bodies that define each reference motion instead of uniformly averaging over the body. Together, STC, TIS, and MPJPE-W provide a more behavior-sensitive view of humanoid tracking than standard SR and MPJPE alone. We believe these metrics are broadly useful for comparing future whole-body controllers in the high-coverage regime, where the remaining differences are often concentrated in threshold sensitivity, motion salience, and long-tail robustness.

Acknowledgements

We sincerely thank Dr. Shidi Li, Zhiyi Rong, Shuaikang Ma, and Dr. Chuanzheng Li for their valuable support of this work and for their extensive contributions to the whole-body control (WBC) framework on which our study was built. Developed through a collaborative effort, the original WBC training infrastructure was shaped in large part by their work on its core design and on the deep reinforcement learning (DRL) implementation for General Motion Tracking (GMT). They also collected and curated the initial motion-capture data and built the associated motion-retargeting pipeline. This shared foundation served as the starting point for our development of Athena-WBC and provided the baseline used in our comparisons, substantially facilitating our research on long-tail humanoid motion tracking.

References

[1] Zhengyi Luo, Ye Yuan, Tingwu Wang, Chenran Li, Fernando Castañeda, Sirui Chen, Zi-Ang Cao, Jiefeng Li, David Minor, Qingwei Ben, Jinhyung Park, David Sami, Zi Wang, Xingye Da, Runyu Ding, Cyrus Hogg, Lina Song, Edy Lim, Eugene Jeong, Tairan He, Haoru Xue, Wenli Xiao, Simon Yuen, Jan Kautz, Yan Chang, Umar Iqbal, Linxi Jim Fan, and Yuke Zhu. SONIC: Supersizing motion tracking for natural humanoid whole-body control, 2025. URL https://arxiv.org/abs/2511.07820.

[2] Zhengyi Luo, Jinkun Cao, Alexander Winkler, Kris Kitani, and Weipeng Xu. Perpetual humanoid control for real-time simulated avatars. In *Proceedings of the IEEE/CVF International Conference on Computer Vision (ICCV)*, pages 10861–10870, 2023. doi: 10.1109/ICCV51070.2023.01000.

[3] Tairan He, Zhengyi Luo, Xialin He, Wenli Xiao, Chong Zhang, Weinan Zhang, Kris M. Kitani, Changliu Liu, and Guanya Shi. OmniH2O: Universal and dexterous human-to-humanoid whole-body teleoperation and learning. In Pulkit Agrawal, Oliver Kroemer, and Wolfram Burgard, editors, *Proceedings of The 8th Conference on Robot Learning*, volume 270 of *Proceedings of Machine Learning Research*, pages 1516–1540. PMLR, 2025. URL https://proceedings.mlr.press/v270/he25b.html.

[4] Chao Yang, Yingkai Sun, Peng Ye, Xin Chen, Chong Yu, and Tao Chen. EGM: Efficiently learning general motion tracking policy for high dynamic humanoid whole-body control, 2025. URL https://arxiv.org/abs/2512.19043.

[5] Zhenguo Sun, Bo-Sheng Huang, Yibo Peng, Xukun Li, Jingyu Ma, Yu Sun, Zhe Li, Haojun Jiang, Biao Gao, Zhenshan Bing, Xinlong Wang, and Alois Knoll. MOSAIC: Bridging the Sim-to-Real

gap in generalist humanoid motion tracking and teleoperation with rapid residual adaptation, 2026. URL https://arxiv.org/abs/2602.08594.

[6] Zhenguo Sun, Yibo Peng, Yuan Meng, Xukun Li, Bo-Sheng Huang, Zhenshan Bing, Xinlong Wang, and Alois Knoll. RobotDancing: Residual-action reinforcement learning enables robust long-horizon humanoid motion tracking, 2025. URL https://arxiv.org/abs/2509.20717.

[7] Zuxing Lu, Ziang Zheng, Yao Lyu, Jingyu Liu, Feihong Zhang, Song Lu, Xin Yuan, Changyin Sun, Xingxing Zuo, and Shengbo Eben Li. M3imic: Learning a versatile whole-body controller for multimodal motion mimicking, 2026. URL https://arxiv.org/abs/2606.04829.

[8] Xiao Ren, Yuhui Yang, Zongbiao Weng, Zhijie Liu, and He Kong. Stubborn: A streamlined and unified reinforcement learning framework for robust motion tracking and fall recovery for humanoids, 2026. URL https://arxiv.org/abs/2606.12814.

[9] Yixuan Pan, Ruoyi Qiao, Li Chen, Kashyap Chitta, Liang Pan, Haoguang Mai, Qingwen Bu, Hao Zhao, Cunyuan Zheng, Ping Luo, and Hongyang Li. Agility meets stability: Versatile humanoid control with heterogeneous data, 2025. URL https://arxiv.org/abs/2511.17373.

[10] Yuxuan Wang, Ming Yang, Weishuai Zeng, Yu Zhang, Xinrun Xu, Haobin Jiang, Ziluo Ding, and Zongqing Lu. From experts to a generalist: Toward general whole-body control for humanoid robots, 2025. URL https://arxiv.org/abs/2506.12779.

[11] Zekun Qi, Xuchuan Chen, Dairu Liu, Chenghuai Lin, Yunrui Lian, Sikai Liang, Zhikai Zhang, Yu Guan, Jilong Wang, Wenyao Zhang, Xinqiang Yu, He Wang, and Li Yi. Humanoid-GPT: Scaling data and structure for zero-shot motion tracking, 2026. URL https://arxiv.org/abs/2606.03985.

[12] Stephane Ross, Geoffrey Gordon, and Drew Bagnell. A reduction of imitation learning and structured prediction to no-regret online learning. In Geoffrey Gordon, David Dunson, and Miroslav Dudík, editors, *Proceedings of the Fourteenth International Conference on Artificial Intelligence and Statistics*, volume 15 of *Proceedings of Machine Learning Research*, pages 627–635, Fort Lauderdale, FL, USA, 2011. PMLR. URL https://proceedings.mlr.press/v15/ross11a.html.

[13] Zixuan Chen, Mazeyu Ji, Xuxin Cheng, Xuanbin Peng, Xue Bin Peng, and Xiaolong Wang. GMT: General motion tracking for humanoid whole-body control, 2025. URL https://arxiv.org/abs/2506.14770.

[14] Jean Pierre Sleiman, He Li, Alphonsus Adu-Bredu, Robin Deits, Arun Kumar, Kevin Bergamin, Mohak Bhardwaj, Scott Biddlestone, Nicola Burger, Matthew A. Estrada, Francesco Iacobelli, Twan Koolen, Alexander Lambert, Erica Lin, M. Eva Mungai, Zach Nobles, Shane Rozen-Levy, Yuyao Shi, Jiashun Wang, Jakob Welner, Fangzhou Yu, Mike Zhang, Alfred Rizzi, Jessica Hodgins, Sylvain Bertrand, Yeuhi Abe, Scott Kuindersma, and Farbod Farshidian. ZEST: Zero-shot embodied skill transfer for athletic robot control, 2026. URL https://arxiv.org/abs/2602.00401.

[15] Yuhan Li, Peiyuan Zhi, Yunshen Wang, Tengyu Liu, Sixu Yan, Wenyu Liu, Xinggang Wang, Baoxiong Jia, and Siyuan Huang. OmniTrack: General motion tracking via physics-consistent reference, 2026. URL https://arxiv.org/abs/2602.23832.

[16] Siddharth Mysore, Bassel Mabsout, Renato Mancuso, and Kate Saenko. Regularizing action policies for smooth control with reinforcement learning. In *2021 IEEE International Conference on Robotics and Automation (ICRA)*, pages 1810–1816, 2021. doi: 10.1109/ICRA48506.2021.9561138.

[17] I. Lee, Hoang-Giang Cao, Cong-Tinh Dao, Yu-Cheng Chen, and I-Chen Wu. Gradient-based regularization for action smoothness in robotic control with reinforcement learning. In *2024 IEEE/RSJ International Conference on Intelligent Robots and Systems (IROS)*, pages 603–610, 2024. doi: 10.1109/IROS58592.2024.10801464.

[18] Zhuang Liu, Xuanlin Li, Bingyi Kang, and Trevor Darrell. Regularization matters in policy optimization – an empirical study on continuous control. In *International Conference on Learning Representations*, 2021. URL https://openreview.net/forum?id=yr1mzrH3IC.

[19] Ashvin Nair, Abhishek Gupta, Murtaza Dalal, and Sergey Levine. AWAC: Accelerating online reinforcement learning with offline datasets, 2020. URL https://arxiv.org/abs/2006.09359.

[20] Ye Yuan and Kris Kitani. Residual force control for agile human behavior imitation and extended motion synthesis. In *Advances in Neural Information Processing Systems*, volume 33, 2020. URL https://proceedings.neurips.cc/paper/2020/hash/f76a89f0cb91bc419542ce9fa43902dc-Abstract.html.

[21] Zhanxiang Cao, Yang Zhang, Buqing Nie, Huangxuan Lin, Haoyang Li, and Yue Gao. Learning motion skills with adaptive assistive curriculum force in humanoid robots, 2025. URL https://arxiv.org/abs/2506.23125.

[22] Nikita Rudin, Junzhe He, Joshua Aurand, and Marco Hutter. Parkour in the wild: Learning a general and extensible agile locomotion policy using multi-expert distillation and RL fine-tuning. *The International Journal of Robotics Research*, 2026. doi: 10.1177/02783649261455067. URL https://doi.org/10.1177/02783649261455067. OnlineFirst.

[23] Naureen Mahmood, Nima Ghorbani, Nikolaus F. Troje, Gerard Pons-Moll, and Michael J. Black. AMASS: Archive of motion capture as surface shapes. In *Proceedings of the IEEE/CVF International Conference on Computer Vision (ICCV)*, pages 5441–5450, 2019. doi: 10.1109/ICCV.2019.00554.

[24] Haiyang Liu, Zihao Zhu, Naoya Iwamoto, Yichen Peng, Zhengqing Li, You Zhou, Elif Bozkurt, and Bo Zheng. BEAT: A large-scale semantic and emotional multi-modal dataset for conversational gestures synthesis. In *Computer Vision – ECCV 2022*, pages 612–630, 2022. doi: 10.1007/978-3-031-20071-7_36.

A Appendix

A.1 Training Hyperparameters

Table 7 lists the PPO and runner settings shared by the ablations.

Table 7: PPO and training hyperparameters.

Hyperparameter	Value
Optimizer	Adam
PPO clip parameter	0.2
Discount factor γ	0.99
GAE parameter λ	0.95
Learning rate	2.0×10^{-5}
Learning-rate schedule	adaptive
Desired KL	0.01
Number of learning epochs	5
Number of mini-batches	4
Value loss coefficient	50.0
Reconstruction loss coefficient	1.0
Token loss coefficient	1.0
Cycle loss coefficient	1.0
Entropy coefficient	0.005
Maximum gradient norm	0.1
Total training environments	16384
Distributed workers	8 GPUs
Training horizon	40k iterations

A.2 Adaptive Motion Sampling

We use adaptive sampling to allocate more rollouts to currently difficult training clips. For each clip τ_m, we divide its timeline into temporal bins $b \in \mathcal{B}_m$ and maintain an online smoothed difficulty score $d_{m,b}$ for each bin. The sampler itself operates at the clip level; bins are used only to detect localized hard phases inside a clip.

For each visited bin, we compute a tracking-difficulty score from three threshold-normalized tracking errors: key-body position, root height, and root heading. Let $\eta^{\text{body}}_{m,b}$, $\eta^{z}_{m,b}$, and $\eta^{\text{yaw}}_{m,b}$ denote these normalized errors. The raw bin score is

$$s^{\text{raw}}_{m,b} = \max\left\{\eta^{\text{body}}_{m,b}, \eta^{z}_{m,b}, \eta^{\text{yaw}}_{m,b}\right\} + c_{\text{viol}} \sum_{\chi\in\{\text{body},z,\text{yaw}\}} \mathbf{1}\left\{\eta^{\chi}_{m,b} \geq 1\right\}, \tag{A.1}$$

where $c_{\text{viol}} = 0.25$. The maximum term selects the most severe tracking component, while the violation term upweights bins whose normalized errors exceed their thresholds. The stored difficulty score is updated with an exponential moving average,

$$d_{m,b} \leftarrow \beta_{\text{ema}} s^{\text{raw}}_{m,b} + (1 - \beta_{\text{ema}}) d_{m,b}. \tag{A.2}$$

The clip difficulty is the maximum difficulty over its temporal bins:

$$D_m = \max_{b\in\mathcal{B}_m} d_{m,b}. \tag{A.3}$$

The rollout probability of clip τ_m is then

$$p_{\text{samp}}(m) = (1-\rho)\frac{\phi(D_m)}{\sum_{j=1}^{M}\phi(D_j)} + \rho\frac{1}{M}, \qquad \phi(D) = \min(D, D_{\max}) + \epsilon. \tag{A.4}$$

Here $D_{\max}$ caps extreme difficulty scores, ϵ prevents zero probability before normalization, and ρ mixes in uniform sampling to preserve full dataset coverage.

This formulation can also be extended to bin-level sampling by assigning probabilities directly to (m, b) pairs and starting episodes near selected hard phases. Unless otherwise stated, we use the clip-level max-over-bin sampler above.

A.3 Calculation of STC, TIS, and MPJPE-W

We use three complementary metrics to evaluate threshold robustness and motion-specific tracking quality: the Success–Tolerance Curve (STC), Threshold-Integrated Success (TIS), and Motion-Salience Weighted MPJPE (MPJPE-W). STC and TIS are computed from the same threshold-based success predicate as the standard success rate, while MPJPE-W modifies standard MPJPE by assigning larger weights to body parts that are more active in the reference motion.

Success predicate. For a policy π evaluated on a dataset $\mathcal{D}$, each reference clip $\tau_m \in \mathcal{D}$ is rolled out R_m times. At rollout r and frame t, let $e^z_{m,r,t}$ denote the root-height error, let $e^{\text{yaw}}_{m,r,t}$ denote the root-yaw error, and let $e^{\text{kb}}_{m,r,t}$ denote the maximum key-body position error. The default success thresholds are

$$\delta^0_z = 0.20 \text{ m}, \qquad \delta^0_{\text{yaw}} = 0.50 \text{ rad}, \qquad \delta^0_{\text{kb}} = 0.50 \text{ m}. \tag{A.5}$$

A rollout is successful only if all three errors remain below their thresholds for the full reference horizon. Equivalently, at threshold scale $s = 1$,

$$S_\pi(m, r; 1) = \mathbf{1}\left[\max_t e^z_{m,r,t} < \delta^0_z \ \wedge\ \max_t e^{\text{yaw}}_{m,r,t} < \delta^0_{\text{yaw}} \ \wedge\ \max_t e^{\text{kb}}_{m,r,t} < \delta^0_{\text{kb}}\right]. \tag{A.6}$$

The standard success rate is then

$$\text{SR}_\pi(1; \mathcal{D}) = \frac{1}{\sum_{\tau_m \in \mathcal{D}} R_m} \sum_{\tau_m \in \mathcal{D}} \sum_{r=1}^{R_m} S_\pi(m, r; 1). \tag{A.7}$$

Success–Tolerance Curve. A single success-rate number evaluates the policy at only one threshold setting. To measure sensitivity to this choice, we compute success rate after scaling all default thresholds by a nonnegative scale factor $s \geq 0$:

$$\delta_z(s) = s\delta^0_z, \qquad \delta_{\text{yaw}}(s) = s\delta^0_{\text{yaw}}, \qquad \delta_{\text{kb}}(s) = s\delta^0_{\text{kb}}. \tag{A.8}$$

Thus, $s = 1$ gives the default success-rate evaluation, $s < 1$ gives a stricter evaluation, and $s > 1$ gives a looser evaluation.

At scale s, the rollout success indicator is

$$S_\pi(m, r; s) = \mathbf{1}\left[\max_t e^z_{m,r,t} < \delta_z(s) \ \wedge\ \max_t e^{\text{yaw}}_{m,r,t} < \delta_{\text{yaw}}(s) \ \wedge\ \max_t e^{\text{kb}}_{m,r,t} < \delta_{\text{kb}}(s)\right]. \tag{A.9}$$

The success rate at scale s is

$$\text{SR}_\pi(s; \mathcal{D}) = \frac{1}{\sum_{\tau_m \in \mathcal{D}} R_m} \sum_{\tau_m \in \mathcal{D}} \sum_{r=1}^{R_m} S_\pi(m, r; s). \tag{A.10}$$

The Success–Tolerance Curve is the success-rate function over threshold scales:

$$\text{STC}_\pi(s; \mathcal{D}) = \text{SR}_\pi(s; \mathcal{D}), \qquad s \geq 0. \tag{A.11}$$

By construction, $\text{STC}_\pi(1; \mathcal{D})$ is exactly the standard success rate under the default thresholds.

Threshold-Integrated Success. To summarize the full STC with a scalar, we use Threshold-Integrated Success:

$$\mathrm{TIS}(\pi;\mathcal{D}) = \int_0^\infty \mathrm{STC}_\pi(s;\mathcal{D})\frac{ds}{(1+s)^2}. \tag{A.12}$$

The weighting function satisfies

$$\int_0^\infty \frac{ds}{(1+s)^2} = 1, \tag{A.13}$$

so $\mathrm{TIS}(\pi;\mathcal{D}) \in [0,1]$, with a perfect tracker obtaining $\mathrm{TIS} = 1$. The weight $(1+s)^{-2}$ places most of the mass on the strict and moderate tolerance regions, while avoiding the need to choose an arbitrary maximum threshold scale.

Motion-Salience Weighted MPJPE. Standard MPJPE averages Cartesian tracking error uniformly over all evaluated joints or key bodies. This can understate errors on the body parts that define a motion, such as the hand in a waving clip or the feet in a jumping clip. MPJPE-W therefore assigns each evaluated point a clip-specific weight based on its motion salience in the reference.

Let $\mathcal{J}$ denote the set of evaluated non-root joints or key bodies. For clip τ_m, let $\tilde{p}^{\mathrm{ref}}_{m,t,j}$ be the reference position of point $j \in \mathcal{J}$ at frame t, expressed in the heading-local root frame. This removes global root translation and heading, so the salience reflects body-part motion relative to the root rather than global locomotion. The cumulative local motion length of point j is

$$M_{m,j} = \sum_{t=1}^{T_m-1} \left\| \tilde{p}^{\mathrm{ref}}_{m,t+1,j} - \tilde{p}^{\mathrm{ref}}_{m,t,j} \right\|_2. \tag{A.14}$$

To avoid overweighting distal points simply because they are farther from the root, we normalize by the root-to-point kinematic path length. Let L_j denote the sum of nominal link lengths along the kinematic tree from the root to point j. The unnormalized salience score is

$$u_{m,j} = \frac{M_{m,j}}{L_j + \varepsilon}, \tag{A.15}$$

where ε is a small numerical constant. The normalized MPJPE-W weight is

$$w_{m,j} = \begin{cases} \dfrac{u_{m,j}}{\sum_{j' \in \mathcal{J}} u_{m,j'}}, & \sum_{j' \in \mathcal{J}} u_{m,j'} > 0, \\ \dfrac{1}{|\mathcal{J}|}, & \sum_{j' \in \mathcal{J}} u_{m,j'} = 0. \end{cases} \tag{A.16}$$

These weights are computed only from the reference motion and are fixed for all policies evaluated on the same clip.

For rollout r of clip τ_m, let $p^{\pi}_{m,r,t,j}$ be the policy-executed Cartesian position of point j, and let $p^{\mathrm{ref}}_{m,t,j}$ be the corresponding reference position. The per-clip MPJPE-W is

$$\text{MPJPE-W}_\pi(\tau_m) = \frac{1}{R_m}\sum_{r=1}^{R_m}\frac{1}{T_{m,r}}\sum_{t=1}^{T_{m,r}}\sum_{j\in\mathcal{J}} w_{m,j}\left\| p^{\pi}_{m,r,t,j} - p^{\mathrm{ref}}_{m,t,j} \right\|_2. \tag{A.17}$$

The dataset-level MPJPE-W is the clip-uniform average

$$\text{MPJPE-W}_\pi(\mathcal{D}) = \frac{1}{|\mathcal{D}|}\sum_{\tau_m \in \mathcal{D}} \text{MPJPE-W}_\pi(\tau_m). \tag{A.18}$$

We report MPJPE-W in millimeters. The metric is used as a motion-salience-aware diagnostic that augments standard MPJPE rather than replacing it.

A.4 Construction of Diagnostic Dynamic and Balance Manifests

We construct the diagnostic dynamic and balance manifests with an automatic, reproducible pipeline rather than manual clip selection. The goal is to obtain two fixed evaluation subsets that are enriched for high-dynamic and balance-critical motions, while remaining disjoint from the held-out Omni evaluation set.

Candidate pool. The source pool is the full training corpus: the curated mocap set `xpeng-mocap` with 234 clips and 11.64 hours, AMASS-train with 7,333 clips and 25.11 hours, Bones-Seed with 46,341 clips and 95.66 hours, and BEAT with 1,574 clips and 43.47 hours. We filter metadata entries by requiring duration at least 2.0 seconds and no duplicate robot-motion file. This produces $55{,}482$ unique candidate training clips.

Automatic recall. For each clip, we concatenate the clip id, action type, action description, robot-motion-file basename, and human-motion-file basename into a lower-cased text string. Keyword matching assigns clips to semantic buckets. The dynamic bucket covers running, jumping, hopping, leaping, and vaulting. The balance buckets cover single-leg support, inversion or hand-supported motion, low-center-of-mass motion, and yoga/static-balance poses. These semantic rules are used only for candidate recall; final ranking also uses motion-derived proxy features.

Motion-proxy features. For recalled clips, we parse the robot-motion CSV file and extract inexpensive proxy statistics. The features include root height and height range, root tilt, inversion ratio, horizontal speed, root angular velocity, left/right foot contact ratios, single-support ratio, flight ratio, non-foot-contact ratio, and high-percentile joint velocity and acceleration. These features are not intended to be exact physical feasibility tests; they provide automatic cues for whether a clip is dynamic or balance-critical.

The proxy features are also used to augment balance recall. A clip can be added to the single-leg bucket if it spends a large fraction of time in single support while moving slowly. It can be added to the inversion bucket if the root is strongly tilted, inverted, or frequently supported by non-foot contacts. It can be added to the low-COM bucket if the root height is low or changes substantially at low speed. Dynamic candidates, in contrast, are required to match the run/jump/hop semantic bucket, so the dynamic manifest is not expanded purely by proxy features.

Scoring and selection. All continuous proxy features are robustly normalized using the fifth and ninety-fifth percentiles over the scored candidate pool. Dynamic clips are ranked by a positive linear score that combines semantic dynamic recall, horizontal speed, joint velocity, joint acceleration, flight ratio, and root angular velocity. Balance clips are ranked by a positive linear score that combines balance semantic recall, inversion cues, single-support ratio, non-foot-contact ratio, root tilt, low root height, and low horizontal speed.

To avoid a narrow manifest dominated by one motion family, we sample using bucket quotas and deduplication. The dynamic pool is divided into run, jump/hop/leap, vault/flip, high-flight, and high-joint-dynamics buckets. The balance pool is prioritized by inversion, single-leg balance, low-COM balance, and yoga/static-balance buckets. The two manifests are made intentionally non-overlapping by excluding run/jump/hop clips from the balance pool. Within each bucket, clips are ranked by the corresponding score and then deduplicated by motion file and family.

Generated manifests and scope. This procedure produces 1000 clips from 133 families and 1000 clips from 396 families. The dynamic manifest is enriched for running, jumping, hopping, leaping, and flight-heavy motions. The balance manifest covers inversion, low-center-of-mass, single-leg, hand-supported, and yoga/static-balance motions.